Comparison of Earth Observing-1 ALI and Landsat ETM+ for Crop Identification and Yield Prediction in Mexico

David B. Lobell and Gregory P. Asner

***Abstract*—This paper presents a comparison of Earth Observing 1 (EO-1) Advanced Land Imager (ALI) and Landsat-7 Enhanced Thematic Mapper Plus (ETM+) images collected over an agricultural region in northwest Mexico. Across 115 fields with a range of cover types, radiance measurements collected by ALI were within 3% of ETM+ for all five common bands. Crop discrimination was significantly improved with ALI compared to ETM+, with an increase from 85% to 95% accuracy for distinguishing maize from wheat fields. This improvement was attributed to the greater SNR in ALI, as well as the unique information content of ALI band 4p (0.84–0.89 μm), which may be due to sensitivity to canopy water content. Yield predictions from reflectance-calibrated data did not reveal significant differences between the sensors. The greatest distinction between ALI and ETM+ was observed in the panchromatic band, with ALI providing more detailed information on inter- and intrafield radiance differences, which show promise for precision agriculture applications. We conclude that ALI meets or exceeds ETM+ performance for agricultural applications evaluated here, thus providing a plausible option for continuity of the valuable Landsat record.**

***Index Terms*—Advanced Land Imager (ALI), Enhanced Thematic Mapper Plus (ETM+), remote sensing.**

I. Introduction

THE LAUNCH of the Earth Observing 1 (EO-1) satellite on November 21, 2000 marked a key phase in the National Aeronautics and Space Administration's (NASA) New Millenium Program, which has the goal of testing advanced technologies for space and earth exploration. Among the three sensors flown on EO-1 was the Advanced Land Imager (ALI), designed to produce images directly comparable to Landsat-7 Enhanced Thematic Mapper Plus (ETM+), but to do so with significant reductions in sensor size, mass, and cost [1]. An important task of the EO-1 mission is, therefore, to compare the performance of ALI and ETM+ and to evaluate the potential for ALI technology to provide continuity of the 30-year Landsat record.

Manuscript received May 17, 2002; revised March 6, 2003. This work was supported by the National Aeronautics and Space Administration (NASA) New Millenium Program under Grant NCC5-480 and Grant NCC5-481, by the NASA New Investigator Program under Grant NAG5-8709, by the National Science Foundation Graduate Research Fellowship, and by the Packard Foundation.

D. B. Lobell is with the Department of Global Ecology, Carnegie Institution of Washington, Stanford, CA 94305 USA and Department of Geological and Environmental Science, Stanford University, Stanford, CA 94305 USA.

G. P. Asner is with the Department of Global Ecology, Carnegie Institution of Washington, Stanford, CA 94305 USA (e-mail: greg@globalecology.stanford.edu).

Digital Object Identifier 10.1109/TGRS.2003.812909

This paper presents a comparison of ALI and ETM+ images collected over an agricultural region in northwest Mexico on January 14, 2002. In addition to comparing the raw data collected by the two sensors, we compared their performance in specific applications relevant to cropland monitoring and management. This latter comparison was important for translating differences in sensor characteristics to measurements relevant to scientific and management end-users. As in all applications, performance gains or losses should be considered along with the associated costs as well as the required precision and accuracy of a given application.

Several specific applications of remote sensing in agriculture have been identified, ranging from total crop area estimates to mapping of within-field moisture and nutrient deficiencies [2]–[6]. In this study, we focused on two especially common and important applications: crop identification and yield estimation. Discrimination of crop types is needed to provide large-scale area estimates, which are often lacking or severely biased in less-developed countries; information on the spatial distribution of crops, which is useful for tracking the transport of nutrients such as nitrogen into groundwater supplies or adjacent aquatic ecosystems [7]; and constraints on crop-specific characteristics such as water and light-use efficiencies, which are variables needed to estimate evapotranspiration and dry matter production [8], [9]. Crop discrimination is most readily achieved using sequences of images acquired throughout the year along with knowledge of the growing season for each crop [10]. However, frequent cloud cover can severely limit image availability in many agricultural regions, thereby creating a need for spectral discrimination within a single multispectral image. This can present a significant challenge, even when crops are observed at different stages in their respective growth cycles.

Yield estimation from remote sensing goes one step further than crop identification, requiring not only information on crop type but also some measurement of crop condition. Typically, remotely sensed estimates of leaf area index (LAI) or the fraction of absorbed photosynthetically active radiation (fAPAR) are used to drive, update, or initialize crop-specific growth models, which often also incorporate soil and meteorological variables [11], [12]. The resulting yield estimates, which may be available months before harvest, provide valuable information to farmers and governments for marketing and trading decisions. Yield maps also provide the ability to identify consistently high or low yielding areas of fields, which can then be used to define separate management units and analyze spatial and temporal patterns in yields for improved understanding of controls over crop production [5], [13].

Fig. 1. ALI panchromatic image of the Yaqui Valley study region. Fields used to compare ALI and ETM+ radiance are delineated by white lines.

II. Methods

A. Study Area

The study was conducted in the Yaqui Valley of northwestern Mexico (27°N, 110°W), a region that covers 225 000 ha between the Sierra Madre Mountains and the Gulf of California (Fig. 1). The majority of the land in this area ($\sim$ 165 000 ha) is sown with spring wheat in late November–December, receives three to five irrigations throughout the growing season, and is harvested in late April–May. Both durum wheat (*Triticum turgidum* L.) and bread wheat (*Triticum aestivum* L.) are widely grown, comprising roughly 85% and 15% of the total wheat area, respectively. The second most common crop is irrigated maize (*Zea mays* L.), which is typically planted on $\sim$ 10 000 ha in September and harvested in late February.

Field observations were made during the week of January 10–16, 2002 to identify crops present on numerous fields within the Valley (locations shown in Fig. 1). A total of 115 fields were geolocated with a global positioning system unit and classified as one of the following cover types (total number of each given in parentheses): alfalfa (3), bare soil (6), bread wheat (18), brocolli (3), chile pepper (5), durum wheat (38), garbanzo (5), lettuce (1), maize (29), orange (1), potato (3), squash (1), and watermelon (2). Durum wheat appeared very similar to bread wheat and was visually discriminated based on its more erectophile leaves and slightly darker color. These fields were also revisited later in the growing season, when differences are more pronounced, to confirm the wheat type classification.

B. Image Collection and Processing

Landsat ETM+ imagery was collected at 10:35 A.M. local time on January 14, 2002, followed 1 min later by acquisition of ALI data. The spectral range and spatial resolution of bands for each sensor are given in Table I. Radiometric and geometric corrections were applied to the ETM+ data at the U.S. Geological Survey Earth Resources Observation Systems (EROS) Data Center.

TABLE I
Band Characteristics for Landsat ETM+ and EO-1 ALI Sensors. n/a = "Not Applicable"

	EO-1 ALI		Landsat ETM+	
Band	Wavelength (μm)	Ground Resolution (m)	Wavelength (μm)	Ground Resolution (m)
1p	0.433 – 0.453	30	n/a	n/a
1	0.45 – 0.515	30	0.45 – 0.515	28.5
2	0.525 – 0.605	30	0.525 – 0.605	28.5
3	0.633 – 0.69	30	0.63 – 0.69	28.5
4	0.775 – 0.805	30	0.78 – 0.90	28.5
4p	0.845 – 0.89	30	n/a	n/a
5p	1.2 – 1.3	30	n/a	n/a
5	1.55 – 1.75	30	1.55 – 1.75	28.5
7	2.08 – 2.35	30	2.09 – 2.35	28.5
Pan	0.48 – 0.69	10	0.52 – 0.90	14.25

The ALI data were calibrated to radiance using a procedure developed at MIT Lincoln Labs [14]. In-flight measurements of dark current and an internal calibrator lamp were used to define an offset and gain for each band, with a different calibration factor for each detector (each sample across track) in each of the four sensor chip assemblies (SCAs). Dead detectors were not removed from the final dataset, resulting in lines of bad data evident in bands 5 and 5p. Another problem in the distributed dataset was misregistration of band 3 in SCA 3. This has been observed in other ALI images [24] and was attributed to a "leaky" pixel correction applied to band 3 of SCA 3. No band-to-band misregistration was evident in band 2 of SCA 4, which also underwent leaky-pixel corrections [14]. Nonetheless, manual selection of ground control points was required to register band 3 to the other SCA 3 bands.

Both the ETM+ and ALI datasets were converted to surface reflectance for the purposes of yield prediction (see below), using the ACORN software program (AIG, Boulder, CO). Both datasets were also georegistered to within one pixel using geographic information systems (GIS) coverages of roads, which were clearly visible in the images (see Fig. 1). For each of the 115 fields shown in Fig. 1, a rectangular region was defined that covered a large portion of the interior of the field, while avoiding field boundaries. This was done to eliminate potential contamination from roads or adjacent fields when comparing the two sensors.

C. Crop Identification

To compare ALI and ETM+ for crop identification, a supervised maximum-likelihood classification (MLC) was performed on each image using all optical bands (not including Landsat thermal band) for each sensor and the three major crops as classes: maize, durum wheat, and bread wheat. On January 14, all three crops exhibited a range of ground cover, canopy density, and developmental stages. Most maize fields had recently reached the flowering stage and showed early signs of senescence associated with postanthesis development. Wheat

fields were still in the preanthesis stage of development, with several fields exhibiting a significant ($\sim$ 20%) fraction of exposed soil. The ability of each sensor to correctly classify crop type was quantified by comparing the training pixels with their predicted classes in an error matrix.

Overall accuracy was defined as the percentage of total pixels used for training that was correctly classified by the MLC. Producer's accuracy was calculated by dividing the number of pixels correctly classified for each crop by the total number of training pixels for that crop, while user's accuracy was the number of correctly classified pixels divided by the total number of classified pixels for that crop. Finally, the kappa coefficient was calculated as a measure of the significance of the classification results relative to chance agreement

$$\text{kappa} = \frac{N \sum_{i=1}^{3} x_{ii} - \sum_{i=1}^{3} (x_{i+} \bullet x_{+i})}{N^2 - \sum_{i=1}^{3} (x_{i+} \bullet x_{+i})} \quad (1)$$

where x_{ii} is the number of observations in row i and column i; x_{i+} is the total number of observations in row i; x_{+i} is the total number of observations in column i; and N is the total number of observations. A kappa value of zero indicates that a classification is no better than random assignment of pixels, while a value of one indicates perfect agreement between training pixels and their prescribed classes [15].

D. Yield Prediction

Yield estimates were derived for maize following the approach of [16], which relies on satellite estimates of fAPAR to constrain a simple crop growth model. fAPAR was calculated in the same manner for both ALI and ETM+, based on the following:

$$\begin{aligned}\text{fAPAR} =& 0.5 \\ &\cdot \left(\frac{\text{NDVI} - \text{NDVI}_{\min}}{\text{NDVI}_{\max} - \text{NDVI}_{\min}} + \frac{\text{SR} - \text{SR}_{\min}}{\text{SR}_{\max} - \text{SR}_{\min}} \right) \\ &\cdot (\text{fAPAR}_{\max} - \text{fAPAR}_{\min}) + \text{fAPAR}_{\min} \end{aligned} \quad (2)$$

where NDVI is the normalized difference vegetation index

$$\text{NDVI} = \frac{\text{NIR} - \text{RED}}{\text{NIR} + \text{RED}} \quad (3)$$

and SR is the simple ratio index

$$\text{SR} = \frac{\text{NIR}}{\text{RED}}. \quad (4)$$

RED and NIR represent reflectance at red and near-infrared wavelengths, respectively, which correspond to bands 3 and 4 in ETM+ and ALI. $\text{NDVI}_{\min}$ and $\text{NDVI}_{\max}$ are defined as the second and 98th percentiles, respectively, of NDVI within the image, while $\text{SR}_{\min}$ and $\text{SR}_{\max}$ are similarly defined based on the SR image. $\text{fAPAR}_{\min}$ and $\text{fAPAR}_{\max}$ are set equal to 0.01 and 0.95, corresponding to the extremes of potential canopy absorption of photosynthetically active radiation (PAR) [17], [18]. While this approach assumes that fields with extreme values of fAPAR (0.01 and 0.95) are observed within the image, our experience is that this requirement is almost always met when working in an agricultural landscape containing both bare fields and fully developed crops. The use of NDVI and SR is based purely on empirical evidence that a simple combination of the two indices performs better than either one alone [16], [18].

TABLE II
REGRESSION STATISTICS FOR AVERAGE RADIANCE IN EO-1 ALI VS. LANDSAT ETM+ FOR COMMON BANDS IN 115 AGRICULTURAL FIELDS. STANDARD DEVIATIONS OF ESTIMATES ARE SHOWN IN PARENTHESES. [a]SLOPE IS SIGNIFICANTLY DIFFERENT FROM 1.0 ($p = 0.05$). [b]OFFSET IS SIGNIFICANTLY DIFFERENT FROM 0.1 ($p = 0.05$)

Band	Slope	Offset	R^2
1	1.00 (0.01)	0.97[b] (0.42)	0.99
2	1.00 (0.01)	0.59 (0.38)	0.98
3	0.95[a] (0.01)	0.99[b] (0.24)	0.98
5	0.97 (0.02)	0.13 (0.10)	0.97
7	0.95[a] (0.01)	0.05[b] (0.02)	0.98

TABLE III
CORRELATION BETWEEN EO-1 ALI BANDS IN 115 AGRICULTURAL FIELDS

Band	1p	1	2	3	4	4p	5p	5	7
1p	--	.99	.93	.93	-.52	-.52	-.47	.74	.87
1	--	--	.96	.96	-.55	-.55	-.49	.76	.89
2	--	--	--	.94	-.48	-.48	-.39	.80	.85
3	--	--	--	--	-.70	-.70	-.60	.77	.96
4	--	--	--	--	--	.99	.95	-.41	-.77
4p	--	--	--	--	--	--	.95	-.41	-.77
5p	--	--	--	--	--	--	--	-.18	-.66
5	--	--	--	--	--	--	--	--	.83

To estimate yield, a time profile of fAPAR based on growing-degree days was adjusted at each pixel to match the computed fAPAR in the January 14, 2002 image. Daily estimates of fAPAR were then multiplied by measured values of incident PAR to compute total growing-season absorption of PAR (APAR). Finally, yield was calculated using field-measured values of light-use efficiency (LUE) and harvest index (HI):

$$\text{Yield} = \text{APAR} \times \text{LUE} \times \text{HI}. \quad (6)$$

The details of this approach are provided in [16]; however, the important aspect for this study is that any differences between yield estimates in ETM+ and ALI were due solely to differences in fAPAR. While the high correlations between the relevant bands (Tables II and III) lead to the expectation of similar yield predictions from the two sensors, quantifying the degree of this similarity is important for translating sensor differences into practical units (e.g., tons per hectare). Unfortunately, field measurements of maize yields were not available for independent validation of yields. We, therefore, assessed the performance of ETM+ and ALI yield predictions relative to each other on the 29 maize fields, and cannot state which are closer to the actual yields. Wheat yields were not considered since the image was acquired too early in the season for accurate yield prediction.

III. RESULTS

A. Multispectral Comparison

Radiance measurements in the five common bands of ETM+ and ALI (bands 1, 2, 3, 5, and 7) agreed very well in the 115 fields surveyed (Table II). These fields spanned a range of cover types from bare soil to fully developed canopies and, therefore, facilitated a comparison of radiance across a wide range of values in each band. Band 1 averaged 2.3% higher in ALI than ETM+, with corresponding values of 1.8%, 0.5%, -0.7%, and -0.8% for bands 2, 3, 5, and 7, respectively. Thus, we conclude

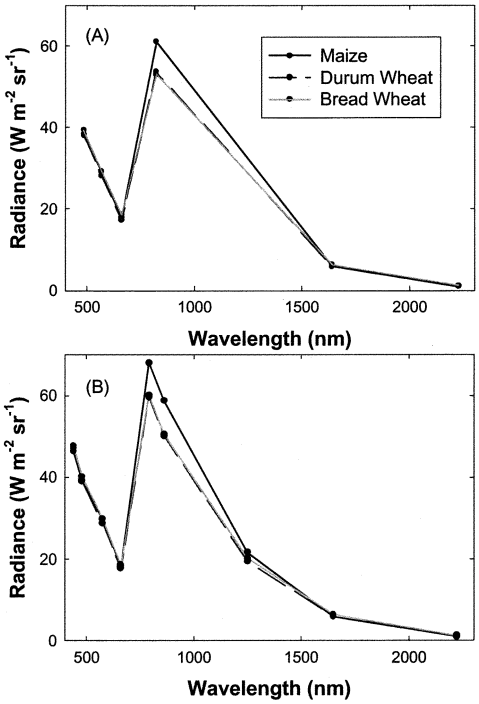

Fig. 2. Average radiance spectra for maize, durum wheat, and bread wheat fields measured by (a) ETM+ and (b) ALI.

that ALI radiance was generally within 2% of ETM+ measurements.

A correlation matrix of ALI bands indicated that bands 1p and 4p were highly correlated with their neighboring bands 1 and 4 (Table III). Band 5p exhibited a slightly negative correlation with band 5 in these fields ($r = -0.18$), and was correlated most strongly with band 4p ($r = 0.95$). Since both ALI bands 4 and 4p were highly correlated with ETM+ band 4 ($r > 0.99$), these results suggest that the "prime" bands in ALI added little additional spectral information over ETM+ data in this setting. However, small differences between highly correlated bands may still represent a significant source of information. The following sections explore the nature of this information for crop identification and yield prediction.

B. Crop Identification

The average radiance spectra for maize, durum wheat, and bread wheat are shown in Fig. 2(a) for ETM+ and Fig. 2(b) for ALI. The most prominent difference between maize and wheat spectra was the magnitude of NIR radiance, reflecting the more advanced stage of canopy development for maize at this time of year, which results in greater scattering of NIR photons. The two wheat spectra were very similar, with the greatest difference observed at band 3 of both sensors. This agrees with field observation of slightly darker leaves in durum wheat.

The results of the MLC are summarized in Table IV for the ETM+ image and in Table V for ALI. Overall classification accuracy increased from 72.0% to 81.4% from ETM+ to ALI, resulting mainly from improved separation of maize from wheat. A classification was also performed using only the ALI bands common to ETM+ (discarding the prime bands), resulting in 78.8% overall accuracy. These results suggest that both the increased SNR of ALI and the additional spectral information in the ALI prime bands, although small in magnitude, have a significant impact on crop classification. In this case, the difference between band 4 and 4p radiance distinguished maize from wheat beyond the capabilities of ETM+ (Fig. 3). While the two bands were highly correlated, maize fields were marked by consistently higher radiance in band 4p relative to wheat fields with the same radiance in band 4.

We attribute this difference to the onset of senescence in maize, which is accompanied by a decrease in canopy water content. Numerous previous studies have shown that the derivative of reflectance near 900 nm increases as leaf water content decreases, because of the strong absorption of water at longer wavelengths [19]–[22]. The sensitivity of ALI to these subtle changes, and the resulting improvements in classification, demonstrates the utility of the multiple NIR bands notwithstanding their extremely high correlation. Although wheat classification was also improved in ALI, this was due mainly to the removal of erroneously classified maize pixels. Significant confusion between durum and bread wheat was evident for both sensors.

TABLE IV
ERROR MATRIX FOR SUPERVISED MAXIMUM LIKELIHOOD CLASSIFICATION OF JANUARY 14, 2002 LANDSAT ETM+ IMAGE. VALUES INDICATE THE NUMBER OF PIXELS OF EACH CROP FALLING IN EACH CLASS

	Training Set Data			
Class	Maize	Durum Wheat	Bread Wheat	Total
Maize	1761	281	41	2083
Durum Wheat	225	1865	193	2283
Bread Wheat	74	944	894	1912
Column Total	2060	3090	1128	6278
Producer's Accuracy (%)	85.5	60.4	79.3	
User's Accuracy (%)	85.5	81.7	46.8	
Overall accuracy = 72.0%; Kappa coefficient = 0.57				

TABLE V
ERROR MATRIX FOR SUPERVISED MAXIMUM LIKELIHOOD CLASSIFICATION OF JANUARY 14, 2002 EO-1 ALI IMAGE. VALUES INDICATE THE NUMBER OF PIXELS OF EACH CROP FALLING IN EACH CLASS

	Training Set Data			
Class	Maize	Durum Wheat	Bread Wheat	Total
Maize	1778	86	0	1864
Durum Wheat	76	1942	169	2187
Bread Wheat	1	712	844	1557
Column Total	1855	2740	1013	5608
Producer's Accuracy (%)	95.9	70.9	83.3	
User's Accuracy (%)	95.4	88.8	54.2	
Overall accuracy = 81.4%; Kappa coefficient = 0.74				

C. Yield Prediction

Although band 4 comprises a more narrow wavelength range in ALI than ETM+, the fAPAR estimates from each sensor were very close, resulting in similar yield predictions (Fig. 4). The root mean square difference between ALI and ETM+ estimates was 0.30 tons ha^{-1}, which is roughly 5% of average yields. Differences in yield estimates from ALI using band 4 versus band

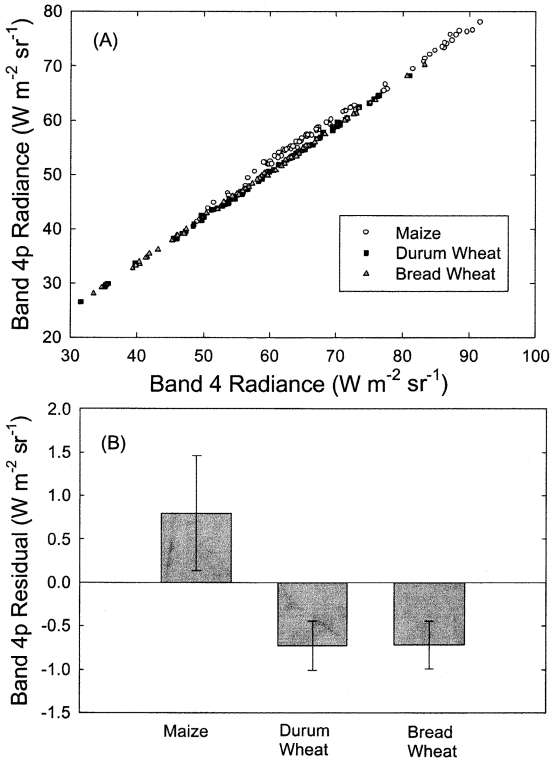

Fig. 3. (a) Scatter plot of radiance in ALI bands 4 and 4p for the three major crops. (b) Mean residuals of the best-fit regression line between bands 4 and 4p. Error bars show one standard deviation from the mean.

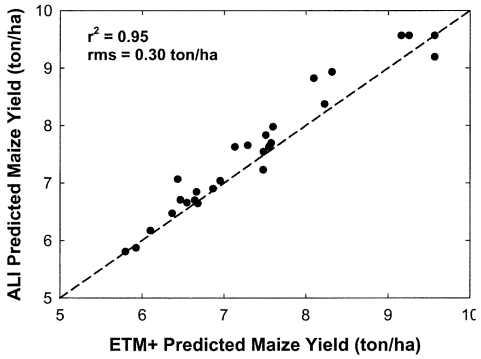

Fig. 4. Comparison of predicted maize yields using ETM+ and ALI sensors for 29 fields. Dashed line is 1 : 1 line.

4p as the NIR band in (2) were less than 1%, which reflects the high correlation between NDVI computed using band 4 versus 4p ($R^2 > 0.99$).

In the absence of field measurements of yield, it is difficult to say which sensor more accurately predicted true yields. However, previous yield estimates for wheat in this region using Landsat ETM+ have proven highly accurate, with errors generally within 0.4 ton/ha [16]. We can conclude here that the differences between the two sensors for yield prediction are small and of secondary importance in the context of other modeling uncertainties [16].

D. Panchromatic Comparison

While this study focused on the multispectral sensors of ETM+ and ALI, the most significant differences were observed in the panchromatic (pan) bands. Fig. 5 shows the pan band of each sensor for a 4×4 km subregion within the Valley. The

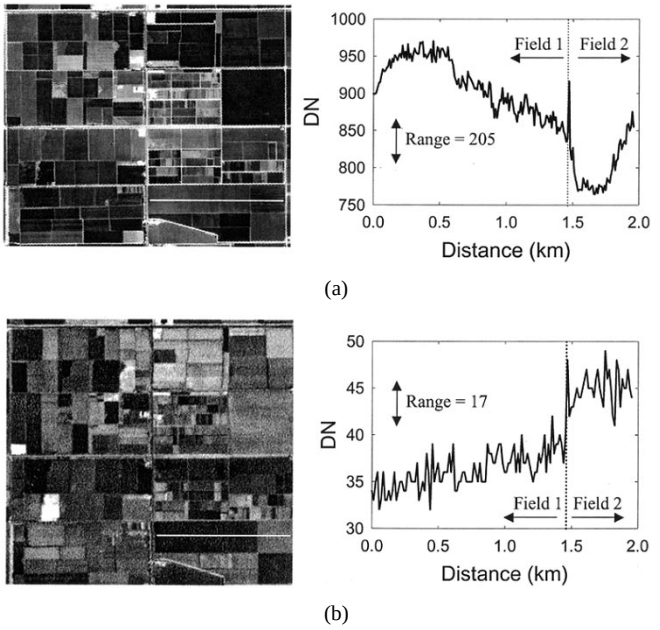

Fig. 5. A panchromatic image from (a) ALI and (b) ETM+ for a 4×4 km area within the study region, demonstrating superior quality of ALI. Digital number (DN) values along the transect indicated by the white line are plotted on the right. The dotted line marks the boundary between two fields.

ALI pan band revealed far more landscape detail than ETM+, as demonstrated by the clear depiction of roads and boundaries between fields.

The enhanced performance of the ALI pan band is attributed to several factors: 1) the instantaneous field of view (IFOV) is 10.0 m versus 14.25 m for ETM+; 2) ALI possesses a superior SNR and a greater dynamic range [23]; and 3) ALI pan is restricted to visible wavelengths (480–690 nm), while ETM+ covers both visible and NIR wavelengths (520–900 nm). The latter aspect is important because multiple scattering by vegetation in the NIR leads to greater pixel-to-pixel interactions, or adjacency effects. Also, sensitivity to both visible and NIR wavelengths reduces the contrast between bare soil and vegetated surfaces for ETM+ relative to ALI (because a decrease in visible reflectance is offset by an increase in NIR reflectance).

The transect in Fig. 5 illustrates the lower SNR and larger dynamic range of the ALI pan band, which was capable of discerning gradients within each field not evident in the ETM+ data. The ability to resolve small differences within fields is of great relevance to precision agriculture (PA), which aims to adjust inputs within fields to account for soil and topographic variations [13]. This ALI image could be used to detect early season deficiencies in different parts of the field, which could then be addressed by the farmer. Significantly, most applications of remote sensing in PA to date have utilized airborne instruments, largely because of the limited spatial resolution of satellite sensors. The availability of low-cost satellite images with a spatial resolution of 10 m could have a great impact on the future of PA, especially for the majority of the world's farmers who cannot afford ground- or airplane-based approaches [13].

IV. Summary and Conclusion

Radiance measurements collected by ALI over an agricultural region agreed very well with coincident Landsat data. The ho-

mogeneous fields and accurate georeferencing possible in this agricultural setting allowed us to compare the spectral response of each sensor without complications due to varying pixel sizes. We conclude that ALI is within 3% of Landsat radiance for all five bands with similar wavelength ranges. However, misregistration of band 3 in ALI SCA 3 presents a significant obstacle to operational image analysis that needs to be resolved.

The additional bands in ALI were highly correlated to existing ETM+ bands in this landscape, yet still contained information leading to significant improvements in crop identification. Specifically, residuals of a regression between bands 4 and 4p provided clear discrimination between maize canopies in early stages of senescence and newly formed wheat canopies. This contrast was attributed to the effect of canopy water status on NIR reflectance derivatives, and indicated a potential for more quantitative estimates of canopy water content from ALI that should be tested in future.

The greatest difference between the two sensors was evident in the panchromatic bands, with ALI clearly outperforming ETM+. The high spatial resolution and quality of ALI's pan band enabled detection of within field gradients in early season wheat conditions that could be used by farmers to define distinct management units. Even simple measures of within field variability, if provided in a timely manner, can have significant impacts of cropland management [13].

Overall, we conclude that ALI technology matches Landsat performance in all aspects, with the exception of problems associated with leaky pixels in band 3. For the agricultural applications investigated here, ALI exceeded Landsat capabilities for crop identification resulting from improved SNRs and additional spectral bands (particularly band 4p), and produced very similar yield predictions. In addition, the ALI panchromatic band provided superior high spatial resolution images owing to its increased *S/N* and dynamic range and its decreased IFOV and spectral range.

ACKNOWLEDGMENT

The authors thank J. I. Ortiz-Monasterio for help collecting information on crop locations and maize light interception, and A. Warner and K. Heidebrecht for assistance with data processing.

REFERENCES

[1] S. G. Ungar *et al.*, "Overview of the Earth Observing 1 (EO-1) mission," *IEEE Trans. Geosci. Remote Sensing*, vol. 41, pp. 1149–1159, June 2003.

[2] W. C. Bausch and H. R. Duke, "Remote sensing of plant nitrogen status in corn," *Trans. ASAE*, vol. 39, pp. 1869–1875, 1996.

[3] R. D. Jackson, "Remote-sensing of vegetation characteristics for farm-management," in *Proc. Soc. Photo-Optical Instrumentation Eng.*, vol. 475, 1984, pp. 81–96.

[4] R. B. Macdonald and F. G. Hall, "Global crop forecasting," *Science*, vol. 208, pp. 670–679, 1980.

[5] M. S. Moran, Y. Inoue, and E. M. Barnes, "Opportunities and limitations for image-based remote sensing in precision crop management," *Remote Sens. Environ.*, vol. 61, pp. 319–346, 1997.

[6] M. S. Moran, A. Vidal, D. Troufleau, J. Qi, T. R. Clarke, P. J. Pinter, T. A. Mitchell, Y. Inoue, and C. M. U. Neale, "Combining multifrequency microwave and optical data for crop management," *Remote Sens. Environ.*, vol. 61, pp. 96–109, 1997.

[7] V. Beaujouan, P. Durand, and L. Ruiz, "Modeling the effect of the spatial distribution of agricultural practices on nitrogen fluxes in rural catchments," *Ecolog. Model.*, vol. 137, pp. 93–105, 2001.

[8] D. B. Lobell, J. A. Hicke, G. P. Asner, C. B. Field, C. J. Tucker, and S. O. Los, "Satellite estimates of productivity and light use efficiency in United States agriculture, 1982–1998," *Glob. Change Biol.*, vol. 8, pp. 722–735, 2002.

[9] C. S. T. Daughtry, K. P. Gallo, S. N. Goward, S. D. Prince, and W. P. Kustas, "Spectral estimates of absorbed radiation and phytomass production in corn and soybean canopies," *Remote Sens. Environ.*, vol. 39, pp. 141–152, 1992.

[10] F. G. Hall and G. D. Badhwar, "Signature-Extendible technology—Global space-based crop recognition," *IEEE Trans. Geosci. Remote Sensing*, vol. 25, pp. 93–103, Jan. 1987.

[11] S. J. Maas, "Use of remotely-sensed information in agricultural crop growth-models," *Ecolog. Model.*, vol. 41, pp. 247–268, 1988.

[12] S. Moulin, A. Bondeau, and R. Delecolle, "Combining agricultural crop models and satellite observations: From field to regional scales," *Int. J. Remote Sens.*, vol. 19, pp. 1021–1036, 1998.

[13] Y. C. Lu, C. Daughtry, G. Hart, and B. Watkins, "The current state of precision farming," *Food Rev. Int.*, vol. 13, pp. 141–162, 1997.

[14] J. Mendenhall and L. Ong, "Introduction to the ALI instrument and data processing," in *Proc. Hyperion and ALI Users Workshop*, 2001.

[15] T. M. Lillesand and R. W. Kiefer, *Remote Sensing and Image Interpretation*. New York: Wiley, 2000.

[16] D. B. Lobell, G. P. Asner, J. I. Ortiz-Monasterio, and T. L. Benning, "Remote sensing of regional crop production in the Yaqui Valley, Mexico: Estimates and uncertainties," *Agricul. Ecosyst. Environ.*, vol. 94, pp. 205–220, 2003.

[17] P. J. Sellers, D. A. Randall, C. J. Collatz, J. A. Berry, C. B. Field, D. A. Dazlich, C. Zhang, and G. D. Colello, "A revised land surface parameterization (SiB2) for atmospheric GCM's. Part 1: Model formulation," *J. Clim.*, vol. 9, pp. 676–705, 1996.

[18] S. O. Los, G. J. Collatz, P. J. Sellers, C. M. Malmstrom, N. H. Pollack, R. S. Defries, L. Bounoua, M. T. Parris, C. J. Tucker, and D. A. Dazlich, "A global 9-yr biophysical land surface dataset from NOAA AVHRR dat," *J. Hydrometeorol.*, vol. 1, pp. 183–199, 2000.

[19] B. C. Gao, "NDWI—A normalized difference water index for remote sensing of vegetation liquid water from space," *Remote Sens. Environ.*, vol. 58, pp. 257–266, 1996.

[20] J. Peñuelas, I. Filella, C. Biel, L. Serrano, and R. Save, "The reflectance at the 950–970 Nm region as an indicator of plant water status," *Int. J. Remote Sens.*, vol. 14, pp. 1887–1905, 1993.

[21] J. Peñuelas, J. Pinol, R. Ogaya, and I. Filella, "Estimation of plant water concentration by the reflectance water index WI (R900/R970)," *Int. J. Remote Sens.*, vol. 18, pp. 2869–2875, 1997.

[22] L. Serrano, S. L. Ustin, D. A. Roberts, J. A. Gamon, and J. Penuelas, "Deriving water content of chaparral vegetation from AVIRIS data," *Remote Sens. Environ.*, vol. 74, pp. 570–581, 2000.

[23] S. G. Ungar, "Comparison of ALI and Landsat data sets," in *Proc. Hyperion and ALI Users Workshop*, 2001.

[24] A. J. Elmore and J. F. Mustard, "Precision and accuracy of EO-1 Advanced Land Imager (ALI) data for semiarid vegetation studies," *IEEE Trans. Geosci. Remote Sensing*, vol. 41, pp. 1311–1320, June 2003.

David B. Lobell received the B.S. degree in applied mathematics from Brown University, Providence, RI, and is currently pursuing the Ph.D. degree at Stanford University, Stanford, CA.

He is currently a Research Fellow at the Department of Global Ecology, Carnegie Institution of Washington, Stanford, CA. His research focuses on the use of remote sensing and modeling to study interactions between land management, soils, and climate in agricultural systems.

Gregory P. Asner received the Ph.D. degree in remote sensing and biogeochemistry from University of Colorado, Boulder.

He is currently a Faculty Member of the Department of Global Ecology, Carnegie Institution of Washington, Stanford, CA, and a Faculty Member of the Department of Geological and Environmental Science, Stanford University, Stanford, CA. His scientific research combines field studies, airborne and satellite remote sensing, and computer modeling to study the effects of land-use change and climate variability on ecosystem functions at the regional scale. He focuses much of his research on the humid tropical forests and deserts of the world.